ACS Sustainable Chemistry & Engineering

Research Article

pubs.acs.org/journal/ascecg

Self-Organized TiO_2/CoO Nanotubes as Potential Anode Materials for Lithium Ion Batteries

M. Madian,*[,†,§,⊥] L. Giebeler,[†,‡] M. Klose,[†] T. Jaumann,[†] M. Uhlemann,[†] A. Gebert,[†] S. Oswald,[†] N. Ismail,[§] A. Eychmüller,[⊥] and J. Eckert[†,‡]

[†]Institute for Complex Materials, IFW Dresden, Helmholtzstraße 20, D-01069 Dresden, Germany

[‡]Institut für Werkstoffwissenschaft, Technische Universität Dresden, Helmholtzstraße 7, D-01069 Dresden, Germany

[§]Physical Chemistry Department, National Research Center, 33 El-Buhouth Street, P.O. Box 12622, Dokki, Giza, Egypt

[⊥]Physical Chemistry/Electrochemistry, Technische Universität Dresden, Bergstraße 66b, D-01069 Dresden, Germany

Supporting Information

ABSTRACT: Electrode material characteristics need to be improved urgently to fulfill the requirements for high performance lithium ion batteries. Herein, we report the use of the two-phase alloy $Ti_{80}Co_{20}$ for the growth of Ti−Co−O nanotubes employing an anodic oxidation process in a formamide-based electrolyte containing NH_4F. The surface morphology and the current density for the initial nanotube formation are found to be dependent on the crystal structure of the alloy phases. X-ray photoelectron spectroscopy analyses of the grown nanotube arrays along with the oxidation state of the involved elements confirmed the formation of TiO_2/CoO nanotubes under the selected process conditions. The electrochemical performance of the grown nanotubes was evaluated against a Li/Li^+ electrode at different current densities of 10−400 $\mu A\ cm^{-2}$. The results revealed that TiO_2/CoO nanotubes prepared at 60 V exhibited the highest areal capacity of ~600 $\mu Ah\ cm^{-2}$ (i.e., 315 $mAh\ g^{-1}$) at a current density of 10 $\mu A\ cm^{-2}$. At higher current densities, TiO_2/CoO nanotubes showed nearly doubled lithium ion intercalation and a Coulombic efficiency of 96% after 100 cycles compared to lower effective TiO_2 nanotubes prepared under identical conditions. The observed enhancement in the electrochemical performances could be attributed to increasing Li ion diffusion resulting from the presence of CoO nanotubes and the high surface area of the grown oxide tubes. The TiO_2/CoO electrodes preserved their tubular structure after electrochemical cycling with only little changes in morphology.

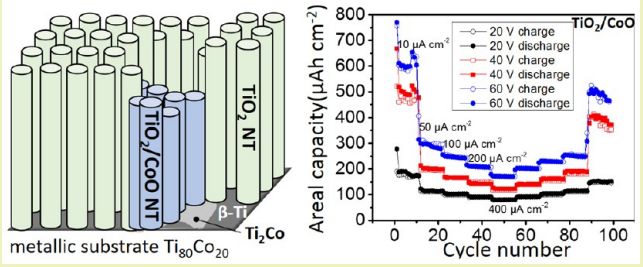

KEYWORDS: *Energy storage, Electrode material, Metal oxide nanotube, Titania nanotube, Cobalt oxide, Ti-based alloy, Anodic oxidation, Nanostructure*

INTRODUCTION

The need for portable power is well established in order to suit all aspects of our modern life. Among all battery systems, lithium ion batteries (LIBs) possess attractive features such as low cost, high theoretical capacity, flexible weight design and long cycle life. Therefore, they are considered as the primary power supply of portable electronic devices and electric vehicles (EVs).[1,2] TiO_2-based anodes are the most promising materials for LIBs to replace carbon due to fast lithium insertion/extraction kinetics, environmentally friendly behavior, low volume change (less than 4%) and therewith high structural stability as well as improved safety issues and low costs.[3−9] These properties are essentially required for employing LIBs in EVs but also in stationary energy storage applications. On the other hand, the low ionic and electric conductivity (≈ 10^{-12} S m^{-1}) of TiO_2 represent the main challenge.[10−12] To improve Li ion diffusion in TiO_2 anodes, an intensive research has been explored in order to reduce its size down to the nanoscale by synthesis of TiO_2 with different nanostructures such as nanoparticles, nanowires and nanotubes, partially mesoporous[6,12−16] or mesoporous incorporated with other materials such as RuO_2,[17] carbon nanospheres[18] and carbon nanotubes (CNTs).[19] Among them, TiO_2 nanotubes fabricated by anodic oxidation are well-aligned, and exhibit uniform tube diameters, wall thicknesses and high surface areas. These properties help to maximize the contact between electrode and electrolyte and to reduce the lithium ion diffusion path.[20−22] Recent research has focused on further improvements of the electronic conductivity of the TiO_2-based nanotubes by doping with other materials such as reduced graphene oxide.[23] Another approach for enhancing the electrochemical performance is found in metal oxide coatings that increase the conductivity within the tube arrays and, in consequence, the specific capacity. As one example for a useful coating of TiO_2, α-MoO_3 is anchored onto the surface of TiO_2 nanotubes, which has improved the lithium ion insertion specific capacities and

Received: January 13, 2015
Revised: March 16, 2015
Published: April 13, 2015

DOI: 10.1021/acssuschemeng.5b00026
ACS Sustainable Chem. Eng. 2015, 3, 909−919

lifetime due to MoO_3 and the stable structure morphology of the TiO_2 nanotubes. The main hurdle for metal oxide coatings on TiO_2 nanotubes is assigned to a slower Li ion migration due to the presence of metal oxide nanoparticles on the nanotube surface.[24]

Alternatively, the fabrication of mixed oxide nanotubes by anodic oxidation of Ti-based alloys is even more promising, as it bundles the advantage to form different metal oxides from one starting material. Due to their interesting properties, various binary and ternary Ti-based systems have recently been explored regarding the formation of mixed oxide nanotubes. Such mixed oxide nanotubes were demonstrated to have real potential for applications. For example, oxide nanotubes obtained from Ti−V, Ti−Ni, Ti−Fe, Ti−Mo−Ni and Ti−6Al−4V alloys were implemented in rechargeable batteries, super capacitors and solar hydrogen production systems, and have been studied under biomedical aspects.[25−29] The Ti−Co−O system is a very promising candidate to contribute significantly to the physicochemical properties such as the relatively high electric and ionic conductivity of CoO to those of TiO_2 beneficial the 1D structures of the formed nanotubes.[30−34] Consequently, the diffusion rate of Li ions through the electrode is expected to be increased. 1D architectures are known to overcome the pulverization or the structure collapse resulting from the large volume changes during lithium ion insertion/extraction.[8] Only recently, Co_3O_4-coated TiO_2 nanotube composites have been formed via a two-step method and improved the conductivity of TiO_2, which therefore improved the lithium storage performance.[35] Moreover, cobalt oxide-modified TiO_2 nanotube arrays showed faster electron transport and highly efficient separation of the photogenerated holes and electrons in the cobalt oxide-anchored TiO_2 nanotubes, which consequently lead to an improvement in visible light photochemical properties.[36]

The main aim of this study is to investigate the possibility to fabricate self-organized Ti−Co−O nanotubes on a current collector of atomic composition $Ti_{80}Co_{20}$ and to study the effect of the presence such mixed oxides on the lithium ion storage for TiO_2 nanotubes. This strategy is expected to improve the electric and the ionic conductivity as well as the reversible capacity of the mixed oxides anode. Moreover, overlapping of CoO with TiO_2 nanotubes in an excellent texture will overcome the structural instability and the resistivity which may result from other synthesis techniques. Furthermore, the nanotubes grown on the substrate, which concurrently serves as a current collector, allows for the good contact between the active materials and the current collector and save the extra cost for binder and additive materials during battery assembly. To the best of our knowledge, no reports have discussed the anodic oxidation of Ti−Co−O or TiO_2−CoO mixed nanotubes in a single step fabrication process because existing procedures just describe impregnation or other deposition processes of TiO_2 nanotubes. The results of this study are promising and expected to be used for developing different research areas such as solar cells and water splitting, but mainly energy storage systems.

EXPERIMENTAL SECTION

Synthesis of TiO_2/CoO and TiO_2 Nanotubes. The $Ti_{80}Co_{20}$ (at. %) prealloy was prepared by arc-melting Ti (99.8%, ARA-T Advance, Germany) and Co (99.9% VEB Mansfeld Kombinat, Germany) metals under argon atmosphere. The prealloy was subsequently cast into rods of 12 mm diameter using a cold crucible device. Discs of 1 mm thickness were cut from the rods and ground with SiC abrasive paper up to grit size P4000 and then polished. Prior to the anodic oxidation, the substrates were sonicated for 30 min in acetone, rinsed with deionized water and finally dried in air. The anodic oxidation experiments of the Ti−Co alloy substrates were realized inside Teflon cells using a programmable DC-power supply (Keithley 2400 source master). A platinum foil was used as the counter electrode and placed at a distance of 1 cm from the Ti−Co alloy substrate used as working electrode. The electrolyte was a formamide-based solution containing 0.2 M NH_4F (99% purity, Merck), 0.1 M H_3PO_4 (85%, Merck) and 3% v/v H_2O.[25] The anodic oxidation experiments were carried out at room temperature applying different voltages (20, 40 and 60 V) for 5 h[37] with a rate of 20 mV s^{-1}. After anodization, the substrates were washed with deionized water and sonicated for a few seconds. The grown nanotubes were thermally treated at 450 °C in air to enhance crystallinity.

Synthesis of TiO_2 Nanotubes. For comparison, TiO_2 nanotube arrays were fabricated from Ti substrates (0.25 mm thick, 99.8% purity, Alfa Aesar) employing the same electrolyte and the anodic oxidation conditions as used for the Ti−Co alloy. The obtained nanotubes were thermally annealed at 450 °C in air.

Structural Characterization. Phase identification of the as-fabricated/annealed nanotubes was performed by X-ray diffraction (XRD, PANalytical X'Pert Pro) using Co Kα radiation and a PIXcel detector in Bragg−Brentano geometry. Field emission scanning electron microscopy (FE-SEM, Gemini LEO 1530, Zeiss) was used to investigate the microstructure of the grown oxide nanotubes. Energy-dispersive X-ray spectroscopy (EDX) analysis were performed to investigate the elemental composition of the as-cast alloy using a Bruker XFlash4010 detector equipped with QUANTAX evaluation software. The chemical composition of the fabricated nanotubes was also explored using X-ray photoelectron spectroscopy (XPS, PHI 5600CI, Physical Electronics). The measurement was carried out at the outer surface of the nanotubes and it is integrating over an area of around 800 μm. Raman spectra of Pure TiO_2 and TiO_2/CoO electrodes were collected using Raman spectroscopy (Thermo Scientific, DXR Smart Raman) with an excitation wavelength of 532 nm at a laser power of 8 mW. The nitrogen sorption experiments were carried out for the annealed nanotubes prepared at 60 V after carefully scratching off the nanotube films from the substrates using a Quantachrome Quadrasorb SI apparatus. Prior to the measurement, the samples were degassed under dynamic vacuum at 150 °C for 24 h. The specific surface areas were calculated in the region of relative pressure p/p_0 = 0.05−0.2 using the multipoint Brunauer−Emmett−Teller (BET) method. The total pore volume was determined at p/p_0 = 0.97. Transmission electron microscopy (TEM) was conducted using a FEI Tecnai F30 with field emission gun at 300 kV acceleration voltage to characterize the electrodes after the electrochemical cycling.

Electrochemical Measurements. Binder and carbon-free electrodes were assembled in an Ar-filled glovebox under controlled O_2 and H_2O content (<0.1 ppm). The electrochemical tests were performed in Swagelok-type cells, in which the anodized TiO_2/CoO nanotubes were used as working electrodes, lithium foil (Alfa Aesar, 99.9%) as counter electrode and standard LP30 (1 M $LiPF_6$, 1:1 DMC/EC, BASF) as electrolyte. All electrochemical measurements were conducted by a multichannel potentiostat/galvanostat (VMP3 potentiostat/galvanostat, Bio-Logic). Cyclic voltammetry tests (CV) were carried out between 1 and 3 V versus Li/Li^+ at a scan rate of 0.1 mV s^{-1}. Swagelok cells were cycled (galvanostatic cycling with potential limitation) at various current densities of 10−400 μA cm^2 between the charge/discharge potentials of 1 and 3 V versus Li/Li^+. The working electrodes consist of thin oxide films of low significant weights, and their applications would be mostly microbatteries, which recommends normalization of the capacity to the area instead of weight. However, the gravimetric capacities are shown in the text. As a reference, TiO_2 nanotubes were assembled and tested at the selected conditions. The average weight of the grown oxide nanotubes was determined after removing the nanotubes from the alloy substrate by sonication in a mixture of ethanol and deionized water (volume ratio 9:1).[5] Three samples from each anodization voltage were weighted

DOI: 10.1021/acssuschemeng.5b00026
ACS Sustainable Chem. Eng. 2015, 3, 909−919

before and after sonication and drying the substrate for 3 h at 120 °C. The electrochemical impedance spectroscopy (EIS) experiments were conducted by a multichannel potentiostat/galvanostat (VMP3 potentiostat/galvanostat, Bio-Logic) after 100 charge/discharge cycles between 100 kHz and 0.1 Hz at a potential of 1.7 V. For postmortem analysis, the cells were disassembled in the glovebox and thoroughly washed with DMC. During transfer to the TEM and the SEM air exposure was minimized.

RESULT AND DISCUSSION

Characterization. The phase composition of the as-cast Ti−Co substrates was investigated by XRD, and the corresponding patterns are shown in Figure 1a. It is clearly shown that the as-cast alloy contains two phases; the first is a β-Ti phase and the second is a Ti_2Co phase. All measured reflections of the two phases are in agreement with the hexagonal structure of β-Ti ($Im\bar{3}m$)[38] and the cubic structure of Ti_2Co ($Fd\bar{3}m$).[39] Other phases such as α-Ti ($P6_3/mmc$)[40] or ω-Ti ($P6/mmm$)[41] may be present in traces. The microstructures of the as-cast $Ti_{80}Co_{20}$ alloy are presented in Figure 1b,c. Two different phases are distributed over the cast sample cross section. The dark areas are related to β-Ti whereas the bright areas represent the Ti_2Co phase. Additionally, the lamellar structure in Figure 1c corresponds to an eutectic mixture of β-Ti and Ti_2Co. EDX element mapping for Ti and Co, as presented in Figure 1d, exhibits the allocation of both Ti and Co with different contents in each phase. According to the phase diagram of the Ti−Co system, the maximum solubility of cobalt in β-Ti and Ti_2Co is ~14% (at 1000 °C) and 33%, respectively, which indicates the possibility to grow mixed oxide nanotubes in both phases.[42]

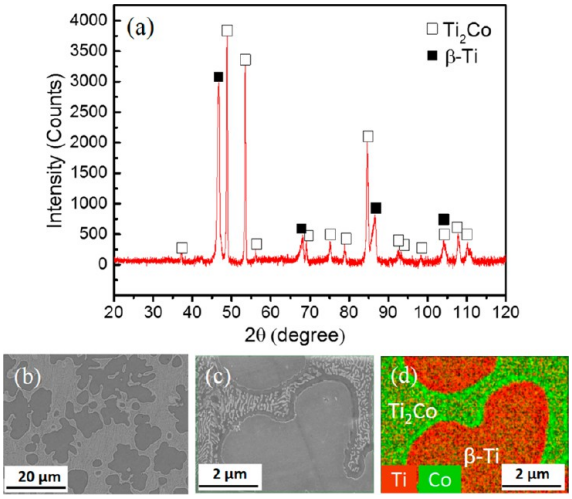

Figure 1. X-ray diffraction pattern (a), SEM micrographs (b,c) and EDX element mapping (d) of the as-cast Ti−Co alloy with green color for the Co signal and red for the Ti signal.

Figure 2a explains the time-current density relationship during the anodic oxidation of $Ti_{80}Co_{20}$ substrates measured at different anodization potentials. At the beginning, the current density rapidly increases due to the growing of metal oxide films. At the peak maximum (P1), the metal surface becomes totally oxidized. Afterward, the drop in the current density occurs because of the passivation effect of the formed oxide layer. Compared to the current density transients of pure Ti (Figure 2b), an additional peak (P2) was observed for $Ti_{80}Co_{20}$ at 10.8 V that corresponds to an anodization time of 9 min. The origin of this peak is related to crack formation as well as to a fresh surface oxidation resulting from an internal surface stress in the β-Ti phase as shown in Figure S1 in the Supporting Information. The stress at the initial stage of the NT growth is attributed to the presence of the two phases, β-Ti and Ti_2Co, with different and unrelated crystal structures. Both phases retain their stability without any cracking before an anodization time of 9 min (Figure S2 in the Supporting Information). After relaxation, the current density decreases due to oxide formation. At point P3, the current density increases again induced by field-assisted chemical dissolution of the oxides by the fluoride ions.[9,27] Ramping periods reaching constant anodization potentials are displayed as R20V, R40V and R60V (Figure 2a). Subsequently, the current density ends in a plateau at steady-state conditions corresponding to an equilibrium between the rate of metal oxidation and chemical etching. It is worth noting that SEM images of the early stage of anodization prove the possibility of growing nanotubes on both alloy phases, as presented in Figures S1 and S2 in the Supporting Information.

Representative images of the Ti−Co alloy microstructures after anodic oxidation are shown in Figure 3. Micrographs a, c and e in Figure 3 represent highly magnified images of the β-Ti phase, whereas micrographs b, d and f correspond to the Ti_2Co phase anodized at 20, 40 and 60 V, respectively. Cross section views in the insets of Figure 3c,d underline the successful fabrication of nanotubes on both phases of the prepared alloy. The nanotubes grown on the β-Ti phase are self-organized, well-aligned and uniform in length. However, the nanotube arrays fabricated on the Ti_2Co phase are distributed irregularly and are defined by much shorter length than those grown on

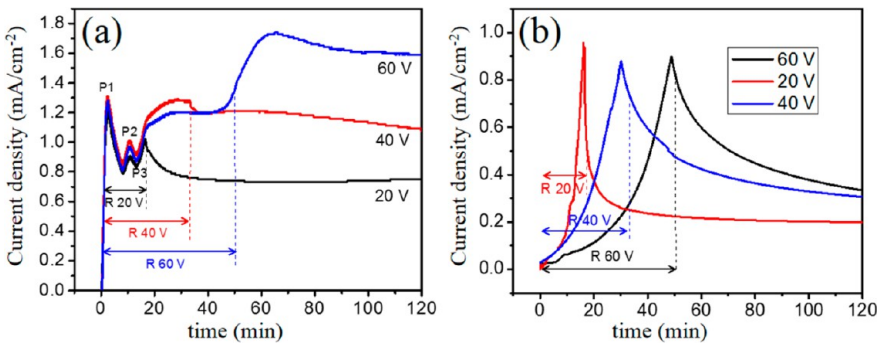

Figure 2. Time-current density relationship of fabricated nanotubes at different anodic oxidation potentials of a $Ti_{80}Co_{20}$ substrate (a) and pure Ti substrate (b).

DOI: 10.1021/acssuschemeng.5b00026
ACS Sustainable Chem. Eng. 2015, 3, 909−919

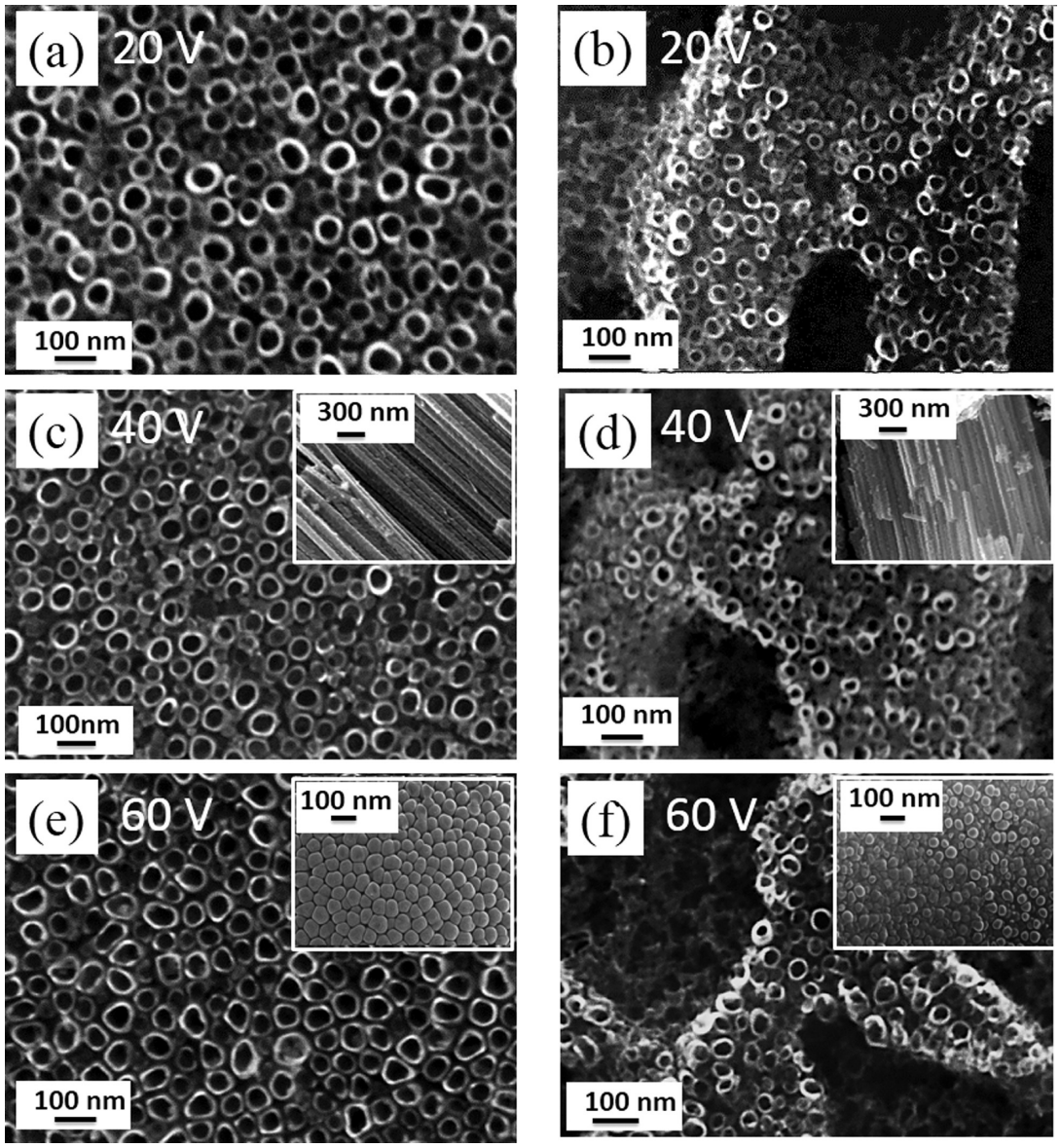

Figure 3. SEM micrographs of the Ti−Co alloy with the β-Ti phase anodized at 20 (a), 40 (c) and 60 V (e), respectively and the Ti_2Co phase anodized at 20 (b), 40 (d) and 60 V (f) for 5 h. Both phases are visible by element contrast and tube growth behavior.

the β-Ti region. The mean lengths of the nanotubes on the β-Ti phase and Ti_2Co after 5 h at 60 V were determined to 27 ± 1 and 24 ± 1 μm, respectively, as presented in Figure S3 in the Supporting Information. A similar behavior was reported for a Ti−6Al−7Nb alloy and was attributed to different etching rates of two different Ti phases during the anodic oxidation.[43] The nanotube diameters and wall thicknesses of both alloy phases are potential independent. For the β-Ti phase, the inner tube diameters are ranging from 37−45 nm. The inner tube diameters of Ti_2Co are smaller than those of the β-Ti phase ranging from 33−40 nm. The thickness of the tube walls of both phases reaches 10 ± 3 nm. The bottom view of the fabricated nanotubes after mechanically scratching off the substrate are shown in the insets in Figure 3e,f inset. The bottoms of the nanotubes grown on both phases are closed. EDX mapping of the anodized alloy in Figure S1 in the Supporting Information showed that the nanotubes formed on the β-Ti phase mainly contain Ti species with some Co whereas the Ti_2Co phase clearly shows both Ti and Co species. From these results, a mixture of TiO_2 nanotubes with CoO nanotubes is deduced for both phases but with differing characteristic and behavior depending on the amount of Co or, later, CoO involved in the anodization process. This difference may be expressed in different growth kinetics of the TiO_2 and the CoO nanotubes, which leads to different tube heights and growth homogeneities, and inhomogeneous alignment on the array. This phenomenon is also observed for various Ti-based alloys[43−45] that contain two phases during the anodic oxidation process. The main reason could be attributed to that the electrolyte may etch one phase easier than the other, which results in that a partial chemical dissolution in one phase and a complete dissolution in the second phase could occur. Consequentially, irregular surface morphologies of the grown nanotube arrays are obtained. The average elemental ratio of the anodized alloy, obtained by EDX analysis, was 86:14 for Ti and Co, respectively, which matches the element content of the as-cast alloy. The different etching rates of the alloy phases can be affected by its atomic ratio. SEM images of TiO_2 nanotubes

DOI: 10.1021/acssuschemeng.5b00026
ACS Sustainable Chem. Eng. 2015, 3, 909−919

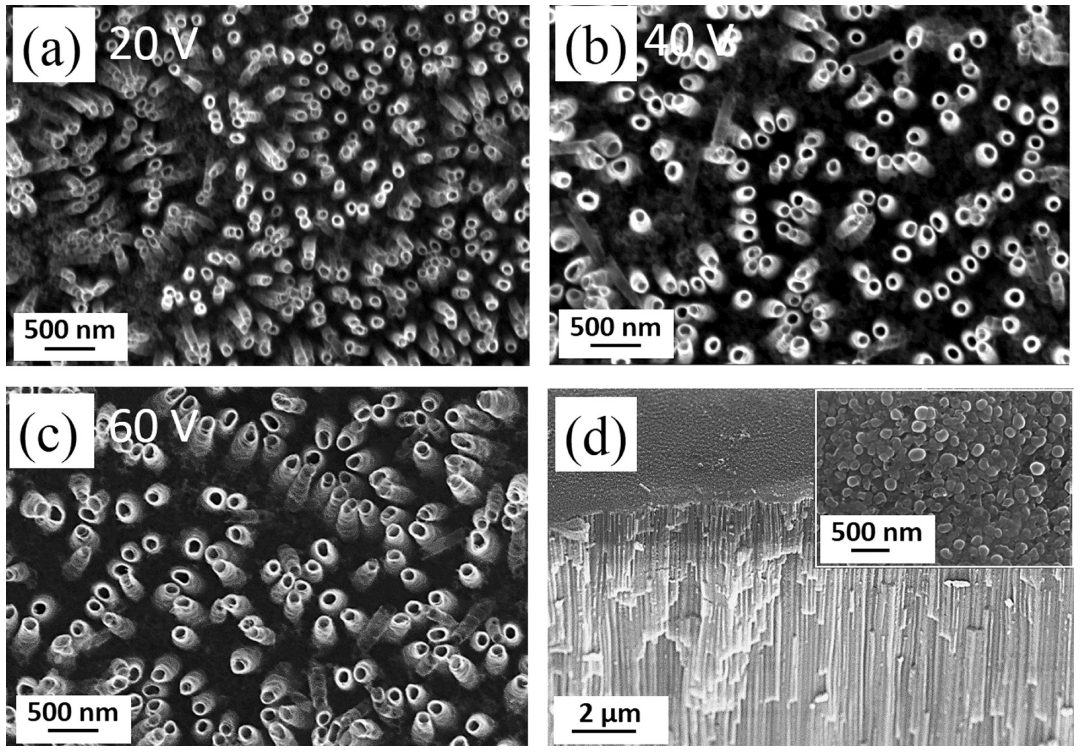

Figure 4. SEM micrographs of the pure Ti, anodized at 20 (a), 40 (b) and 60 V (c), respectively. Cross-sectional view for the sample treated at 60 V (d). The inset in panel d shows the nanotube bottoms.

fabricated under identical anodic oxidation conditions at 20, 40 and 60 V are presented in Figure 4a,b,c, respectively. The growth of the nanotube diameters is proportional to the formation voltage, which is in agreement with the literature.[14] The mean nanotube diameters measured are 75, 105 and 130 nm for the samples prepared at 20, 40 and 60 V, respectively. Image d in Figure 4 shows the tubular structure of the formed tubes, which are closed at the bottoms as seen in the inset. The average nanotubes lengths for the TiO_2 nanotubes formed at 60 V are determined to be 26 ± 1 μm, as presented in Figure S3c in the Supporting Information. Compared to the β-Ti phase on the Ti−Co alloy, the nanotubes grown on the Ti substrate exhibit small gaps between the tube walls. Therefore, the contact between the neighboring nanotubes is lower than for the nanotubes formed on the β-Ti phase of the Ti−Co alloy. From the more intense contact of the tubes formed on the Ti−Co alloy, a better ion transfer and therewith a better kinetic are expected in the electrochemical measurements described below.

The structural characterization of the obtained nanotubes on the Ti−Co alloy was performed using X-ray diffraction, and patterns are presented in Figure 5a. Due to the absence of specific reflections, no hint on the growth of a crystalline oxide film is found. An amorphous state or a very low degree of crystallization is concluded from this observation before annealing. To enhance the crystallinity, the as-anodized substrates were subjected to a thermal treatment for 3 h at 450 °C in air with a heating rate of 1 °C min^{-1}. For the annealed substrates, reflections are observed at 2Θ = 29.5° corresponding to the 011 reflection of the tetragonal anatase phase ($I4_1/amd$).[46] An additional reflection is found at 2Θ = 32° that is related to the 110 reflection of the tetragonal rutile structure ($P4_2/mnm$).[47] Moreover, the signal appearing at 2Θ = 42.7° is assigned to the 101 reflection of hexagonal CoO ($P6_3mc$), confirming the formation of an additional oxide

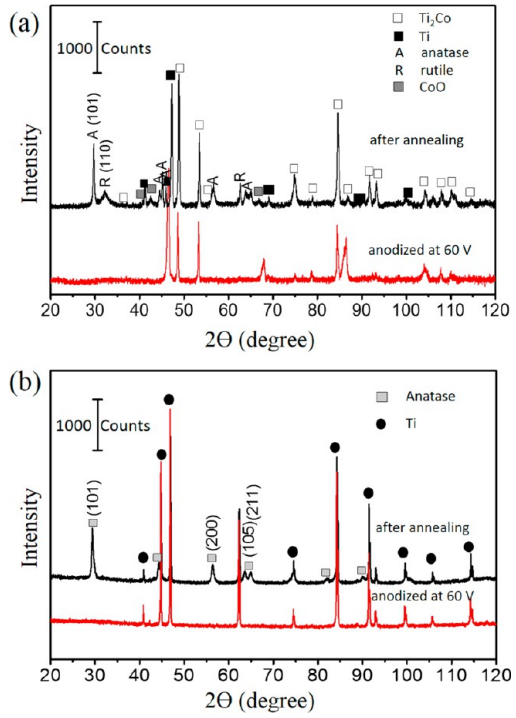

Figure 5. X-ray diffraction patterns of the anodized alloy substrate at 60 V before and after annealing (a) and the anodized Ti substrate treated at 60 V before and after annealing (b).

phase.[48] After the thermal treatment, the reflections of the β-Ti phase are diminished and the reflections of α-Ti appeared. This behavior could be due to separation of cobalt from the β-Ti phase by oxidation and oxide formation. The cobalt concentration together with temperature may not reach

DOI: 10.1021/acssuschemeng.5b00026
ACS Sustainable Chem. Eng. 2015, 3, 909−919

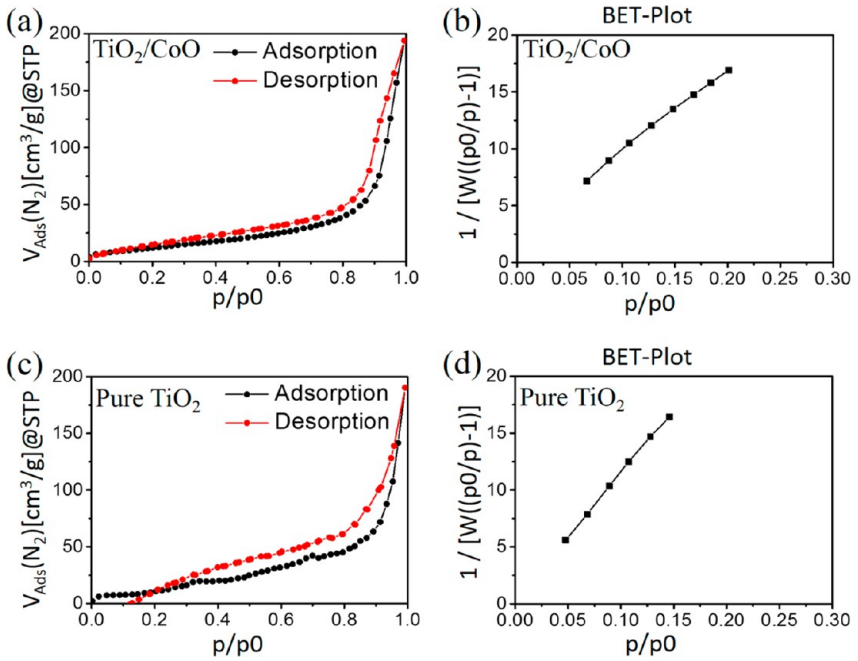

Figure 6. Nitrogen-sorption analysis for the TiO_2/CoO (a,b) and pure TiO_2 NT (c,d), anodized at 60 V.

formation temperature and necessary composition of the β-Ti and ends α-Ti is established. In the X-ray pattern of the anodically oxidized and the annealed sample (Figure 5a), this separation can be recognized as the reflection at 67.5° 2Θ splits into reflections corresponding to CoO and α-Ti. Figure 5b shows the XRD patterns for the as-grown nanotubes on the Ti substrate. The strong 101 reflection was observed for the pure Ti corresponding to the α-Ti phase ($P6_3/mmc$).[40] No noticeable reflections for TiO_2 were observed, indicating the as-formed nanotubes are amorphous. Obvious reflections were identified for the tetragonal anatase phase ($I4_1/amd$)[49] after annealing the formed nanotubes at 450 °C in air.

Nitrogen physisorption experiments were carried out in order to determine the porosity and the specific surface area of the samples. In both cases, the nitrogen adsorption and desorption isotherms shown in Figure 6a,c exhibit type-H1 shapes, which are considered to be indicative for the presence of mesopores (2 nm < d < 50 nm). This result is in accordance with the observations from SEM investigations (Figure 3). In addition, the voids between individual tubes or bundles thereof can be viewed as macropores (d > 50 nm), thus leading to the quickly increasing amount of adsorbed nitrogen in the high-pressure regions of the isotherms.

The BET method was used to determine the specific surface area of the samples, revealing a higher specific surface area and a larger pore volume for TiO_2/CoO nanotubes (46 m^2 g^{-1} and 0.19 cm^3 g^{-1}) in comparison to pure TiO_2 nanotubes (38m^2 g^{-1} and 0.16 cm^3 g^{-1}). The respective BET plots of TiO_2/CoO and pure TiO_2 nanotubes can be found in Figure 6b,d, respectively.

To elucidate the chemical composition of the grown nanotubes on the Ti−Co alloy, we performed XPS analyses. The spectra of the annealed nanotubes are presented in Figure 7a−d. Charging effects of the samples make corrections to the binding energy (BE) scale necessary. The Ti 2p spectra (Figure 7a) showed no broadening and are similar in shape as that reported for TiO_2,[25,27] thus we can deduce that titanium is present as tetravalent Ti. The observed peak of Ti $2p_{3/2}$ is

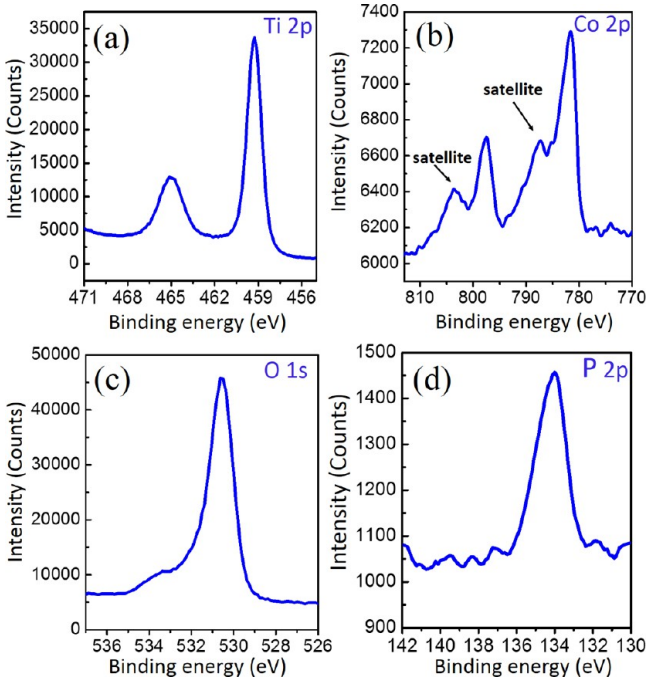

Figure 7. X-ray photoelectron spectra of the grown nanotubes on the Ti−Co alloy at 60 V after annealing for the binding energies Ti 2p (a), Co 2p (b), O 1s (c) and P 2p (d).

therefore suited for BE referencing. Consequently, the Ti $2p_{3/2}$ signal was shifted to 459 eV. Strong Co 2p peaks are observed at 781.5 and 797.5 eV with a spin−orbit splitting of 16 eV that agrees well with the Co 2p signal of CoO[50] with no indication for metallic cobalt (Figure 7b). The shakeup satellite peaks are usually situated 6 eV above the main peak of Co 2p.[51] It has been widely discussed in the literature that the satellite structure at this BE value is characteristic for divalent cobalt in CoO.[51] The observed O 1s peak at 531 eV is another indication for the presence of metal oxides[27] and at 533.2 eV

DOI: 10.1021/acssuschemeng.5b00026
ACS Sustainable Chem. Eng. 2015, 3, 909−919

for hydroxyl groups[52] (Figure 7c). The P 2p peak in Figure 7d appears at 134.2 eV, indicating a pentavalent-oxidation state of an oxygen-bound cationic phosphorus species.[53] Phosphorus remains chemically sorbed on the surface of the nanotubes with a content of about 1 at. % from H_3PO_4 due to its presence in the anodic oxidation bath. From these results, successful formation of TiO_2/CoO nanotube films from a Ti−Co alloy is deduced but mixed Ti−Co−O nanotubes cannot be excluded. The latter is possible because TiO_2 always assimilates certain amounts of other, especially transition metal, elements.

To provide further details about the vibration properties of the fabricated oxide nanotubes, we have performed Raman scattering investigation as another effective characterization tool. Figure 8 shows Raman spectra of the pure TiO_2 and

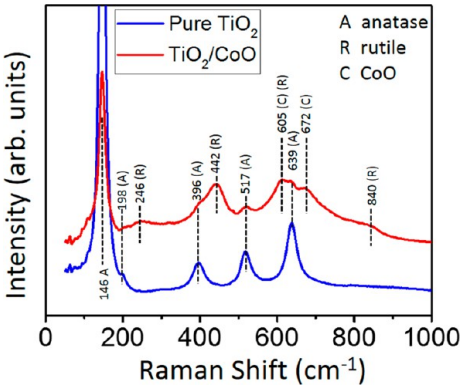

Figure 8. Raman spectra of the pure TiO_2 and TiO_2/CoO grown at 60 V after annealing.

TiO_2/CoO nanotubes, grown at 60 V after annealing. Five pronounced peaks located 146, 198, 396, 517 and 639 cm^{-1} are clearly seen in all spectra. These peaks are assigned to the E_g, E_g, B_{1g}, A_{1g} and E_g vibration modes, respectively of the tetragonal anatase of TiO_2.[54−56] The Raman spectrum of the TiO_2/CoO nanotubes exhibits two additional peaks at ca. 672 and ca. 605 cm^{-1} match those of CoO.[57,58] Note three peaks appeared at 246, 442 and 840 cm^{-1}, which are characteristic of multiphoton process, E_g and B_{2g} modes of rutile phase f TiO_2.[59] Moreover, the ca. 605 cm^{-1} peak could also be associated with that reported for rutile[55] (610 cm^{-1}) with a slight Raman shift of 5 cm^{-1}. The Raman analysis is in a good agreement with XRD and XPS, indicating the successful formation of TiO_2/CoO nanotubes.

ELECTROCHEMICAL TESTING

Cyclic Voltammetry Tests. Cyclic voltammograms of TiO_2 nanotubes and TiO_2/CoO nanotubes formed at 60 V after annealing at 450 °C are shown in Figure 9a,b, respectively. Both samples were tested between 1 and 3 V at a scan rate of 0.1 mV s^{-1} versus Li/Li^+ electrode. Lithium ions easily intercalate into tetragonal anatase by solid state diffusion to yield in orthorhombic Li_xTiO_2 according to eq 1 where $0 \leq x \geq 1$.[60]

$$x\mathrm{Li}^+ + \mathrm{TiO}_2 + x\mathrm{e}^- \leftrightarrow \mathrm{Li}_x\mathrm{TiO}_2 \quad (1)$$

For the TiO_2 sample, anodic and cathodic peaks are located at 1.64 and 2.24 V versus Li/Li^+, respectively, and are typically ascribed to lithium insertion and extraction from the anatase phase (Figure 9a). The presence and almost identical height of the peaks in both the oxidic and reductive branch of the cyclic voltammograms indicates the reversible Li^+ insertion and extraction. The potential separation between the anodic and cathodic peaks in the voltammogram is 0.6 V. For the annealed TiO_2/CoO nanotubes sample (Figure 9b), a pair of anodic/cathodic peaks is observed at 1.7 and 2.06 V versus Li/Li^+, respectively. Two irreversible cathodic peaks present at 1 and 1.4 V appear in the first cycle, which could be attributed to the formation of a stable solid electrolyte interface (SEI). Compared to the TiO_2 electrode, the potential difference between the anodic and cathodic peaks is 0.36 V, which is much lower than that of the TiO_2 electrode. This remarkable reduction in the voltage separation for TiO_2/CoO nanotubes is an indication for better reversibility as well as faster Li^+ diffusion as reported in the literature.[5] Therefore, larger lithium ion storage is expected for the TiO_2/CoO nanotubes sample.

Galvanostatic Cycling. Galvanostatic discharge (lithium insertion) and charge (lithium extraction) measurements were carried out between 1 and 3 V versus Li/Li^+. Figure 10a displays the charge/discharge curves at a current density of 50 $\mu A\ cm^{-2}$ for both TiO_2/CoO and pure TiO_2 samples formed at 60 V, and the inset of Figure 10a represents the corresponding Coulombic efficiency. The TiO_2/CoO electrode showed initial discharge/charge capacities of 435/325 $\mu Ah\ cm^{-2}$ (i.e., 229/171 mAh g^{-1}) with Coulombic efficiencies of ~75%. The initial discharge/charge capacities of the pure TiO_2 electrode reach 250 and 182 $\mu Ah\ cm^{-2}$ (i.e., 150/109 mAh g^{-1}) corresponding to a Coulombic efficiency of around 72%. The irreversible capacity noticed in the first cycle could be ascribed to the formation of a stable solid electrolyte interface (SEI) due to the interaction between the electrolyte and the electrode material.

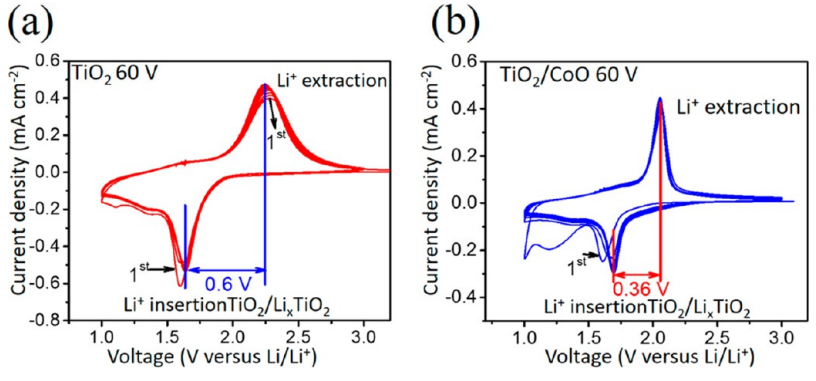

Figure 9. Cyclic voltammograms of TiO_2 (a) and TiO_2/CoO nanotubes (b), prepared at 60 V, measured at scan rates of 1 mV s^{-1}.

DOI: 10.1021/acssuschemeng.5b00026
ACS Sustainable Chem. Eng. 2015, 3, 909−919

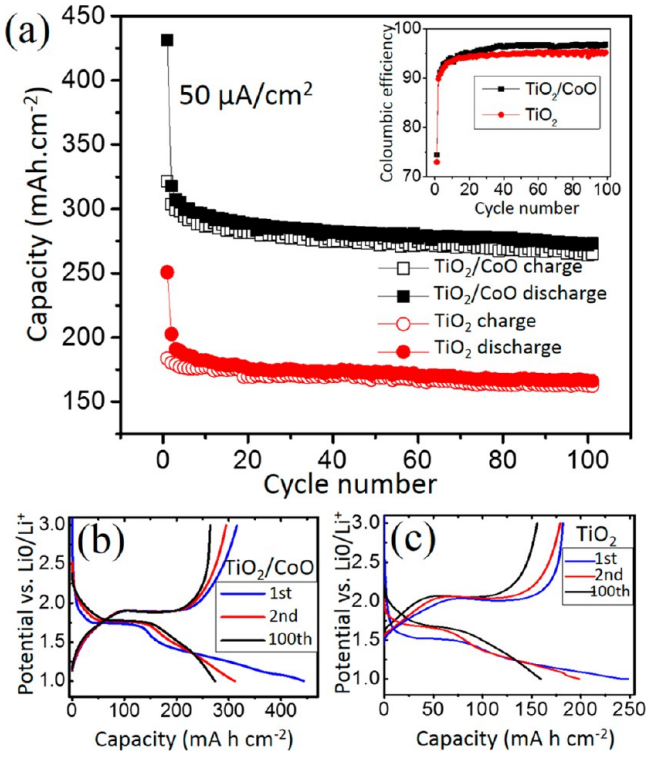

Figure 10. Galvanostatic areal charge and discharge capacities as a function of cycle number obtained at a current density of 50 μA cm^{-2} for pure TiO_2 (a, red circles) and TiO_2/CoO anodes (a, black squares) prepared at 60 V anodization voltages. The filled symbols stand for the discharging and open symbols for the charging processes. The inset shows the corresponding Coulombic efficiency. Typical voltage profiles for the 1st, 2nd and 100th cycles against areal capacity for pure TiO_2 (b) and TiO_2/CoO anodes (c), respectively.

Figure 10b,c shows the voltage profiles of the first, second and 100th discharge/charge cycles for the TiO_2/CoO and the pure TiO_2 electrode, respectively. During the first cycle, the discharge voltage decreases gradually from the open circuit voltage versus Li/Li$^+$ until a plateau at 1.78 V is reached, attributed to the phase transition from the tetragonal anatase and the orthorhombic Li_xTiO_2 due to lithium insertion.[61] The potential continue to decrease to reach their initial capacities afterward. After 100 discharge/charge cycles, TiO_2/CoO was still able to deliver a discharge capacity of 280 μAh cm^{-2}, which is 1.6 times higher as compared to the pure TiO_2 nanotube sample (160 μAh cm^{-2}) and a capacity retention of about 88%.

To demonstrate the electrochemical rate capability, both electrodes were examined with Li ion insertion and extraction at different current densities from 10 to 400 μA cm^{-2}, as presented in Figure 11. It is interesting to note that the areal capacity of each sample is directly proportional to its formation voltage which is related to their weights. It is reported that the tube heights increase by increasing the anodization voltage at constant time using the same electrolyte.[62,63] Therefore, the oxide layer thickness is related to its weight. The TiO_2/CoO electrode, prepared at 60 V (Figure 9b), demonstrated the highest areal capacity of about 600 μAh cm^{-2} (i.e., 315 mAh g^{-1}) at a current density of 10 μA cm^{-2} with cyclic stability up to 83%. The remarkable better rate capabilities of TiO_2/CoO electrode means that it carries more potential for practical applications compared to pure TiO_2 (Figure 11b) formed under the identical conditions. The obtained areal capacity of TiO_2/CoO electrodes in our study are significantly higher than some previously reported values for other systems containing TiO_2 nanotube-based array electrodes such as TiO_2/Fe_2O_3 and MoO_3-deposited TiO_2[24,64] and comparable with the areal capacity of similar system such as for Co_3O_4-coated TiO_2 evaluated at a current density range of 100−200 μA cm^{-2}.[35]

The improved electrochemical performance of TiO_2/CoO nanotubes could be ascribed to the high surface area of the mixed oxide nanotubes with high aspect ratio, i.e., small diameter and long length, compared to pure TiO_2. It is known that the electrochemical performance of TiO_2 nanotubes depends on their specific surface area.[61,65] The specific surface area (S_{BET}) calculated from nitrogen adsorption isotherms showed a higher apparent S_{BET} as well as a larger total pore volume of the TiO_2/CoO nanotubes, (46 m^2 g^{-1} and 0.19 cm^3 g^{-1}) compared to pure TiO_2 nanotubes (37.61 m^2 g^{-1} and 0.16 cm^3 g^{-1}), respectively. The smaller tube diameter and wall thickness of TiO_2/CoO, compared to pure TiO_2, leads to an increase of the specific surface area and a decrease of the Li ion diffusion length. Also, the tube wall contact in TiO_2/CoO is higher than that of pure TiO_2, as confirmed by SEM images, which allows for better ion transfer and higher conductivity. Moreover, an enlargement of the internal surface area of the fabricated tubes may stimulate their capacitive surface for lithium storage, resulting in pseudocapacitance.[66,67] To understand further the reason behind the superior electrochemical performance of the TiO_2/CoO electrode, we performed

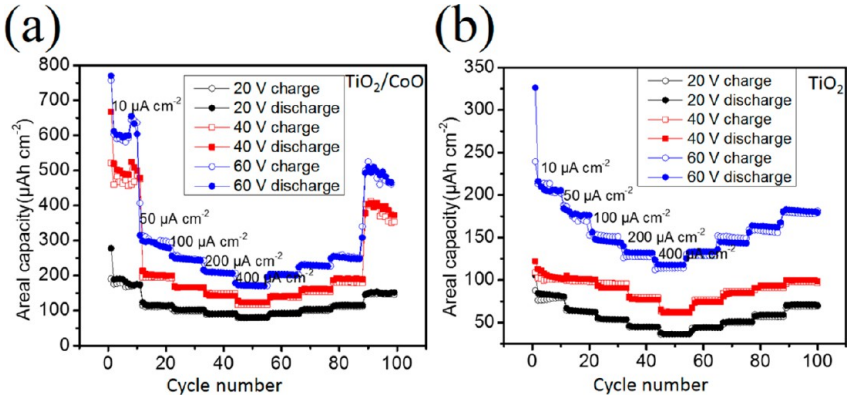

Figure 11. Rate capability of TiO_2/CoO (a) and TiO_2 anodes (b), prepared at anodization voltages of 20 V (black circles), 40 V (red squares) and 60 V (blue circles), as a function of cycle number. The filled symbols explain the discharging and open symbols for the charging processes.

DOI: 10.1021/acssuschemeng.5b00026
ACS Sustainable Chem. Eng. 2015, 3, 909−919

electrochemical impedance spectroscopy (EIS) tests for both the pure TiO_2 and the TiO_2/CoO sample after conducting 100 charge/discharge cycles. The Nyquist plots, for the samples measured at 1.78 V, are presented in Figure 12. Both samples

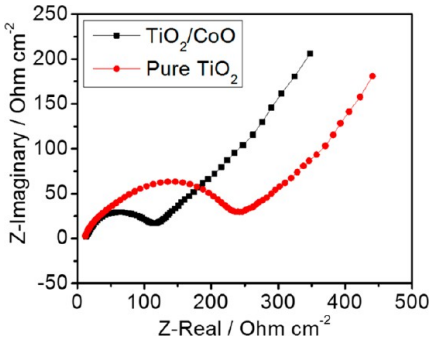

Figure 12. Nyquist plots of TiO_2 (red circles) and TiO_2/CoO anodes (black squares) after conducting 100 charge/discharge cycles, in the frequency range of 100 kHz to 0.1 Hz at a potential of 1.7 V vs Li/Li^+.

exhibit semicircles from high to medium frequency and an inclined line at low frequency region. Such semicircles describe the charge transfer resistance when lithium ions diffuse from the electrolyte into the electrode interface.[22,68] Lithium diffusion from the electrode into the electrolyte is represented by the inclined line. A significant decrease of the semicircle diameter for TiO_2/CoO compared to pure TiO_2 was observed. The presence of CoO positively affects the conductivity of TiO_2, resulting in faster kinetics for lithium ion insertion/extraction processes and better electrochemical performance.

SEM and TEM investigations after 100 charge/discharge cycles at a current density of 400 $\mu A\ cm^{-2}$ are conducted to investigate the morphological stability of the TiO_2/CoO NT upon cycling. Image a in Figure 13 shows the top overview at low magnification of the TiO_2/CoO electrode (prepared at 60 V). Some fibers appeared on the surface, which could be from the separator materials. At a high magnification, the NTs grown on both the β-Ti (Figure 13b) and the Ti_2Co (Figure 13c) phases of the electrodes were maintained their tubular shape without discernible collapse on the nanotube walls. Nevertheless, the nanotube features of the cycled electrode are slightly changed compared to the as-prepared nanotubes (Figure 3). Moreover, the TEM image in Figure 13d shows a marginal deformation of the nanotube.

CONCLUSIONS

In this work, we have investigated the electrochemical growth of well-aligned titanium and cobalt oxide nanotubes on the two-phase alloy $Ti_{80}Co_{20}$. Different voltages (20−60 V) during the anodic oxidation process do not affect the mean nanotube diameters. The current density changes during the dynamic anodization processes and correlates with the morphology depending on the crystal structure of the two phases. The crystallinity of the fabricated oxides was tuned by heat treatment at 450 °C. The structural and spectroscopic characterizations of the oxide films confirm the formation of TiO_2/CoO mixed nanotubes. TiO_2/CoO nanotube anodes displayed a 1.6 times increased areal capacity compared to pure TiO_2 nanotube anodes fabricated under the identical conditions with a capacity retention of 88% over 100 cycles. The improved electrochemical performance of TiO_2−CoO nanotubes is

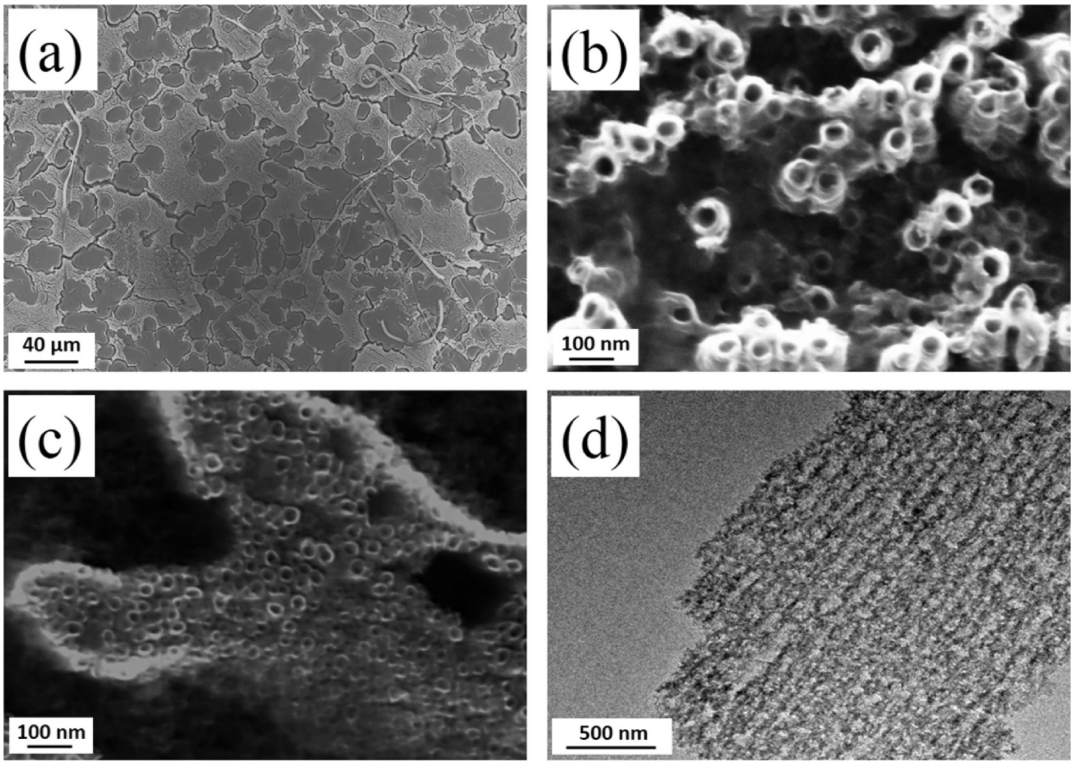

Figure 13. Morphological characterization of the TiO_2/CoO electrode formed at 60 V after 100 charge/discharge cycles at a current density of 400 $\mu A\ cm^{-2}$; SEM images of the top view of the electrode (a); nanotubes grown on the β-Ti phase (b) and Ti_2Co phase (c), respectively; TEM image (d).

DOI: 10.1021/acssuschemeng.5b00026
ACS Sustainable Chem. Eng. 2015, 3, 909−919

attributed to the following reasons: (1) the high surface area of the TiO_2/CoO mixed nanotubes, and (2) the presence of CoO leading to improved conductivity of TiO_2. Such improvement essentially facilitates the Li ion insertion and enhances its reversible capacity. The tubular structure of the TiO_2−CoO nanotubes is well-retained even after electrochemical cycling.

■ ASSOCIATED CONTENT

Supporting Information

Additional SEM images of the early stage of anodization prove the possibility of growing nanotubes on both alloy phases. This material is available free of charge via the Internet at http://pubs.acs.org/.

■ AUTHOR INFORMATION

Corresponding Author

*M. Madian. E-mail: m.madian@ifw-dresden.de. Telephone: +4935146591854. Fax: +493514659452.

Notes

The authors declare no competing financial interest.

■ ACKNOWLEDGMENTS

The European Union (ERDF) and the Free State of Saxony are gratefully acknowledged within the project LTA4ITM (grant no. 100096881) for financial support. M.M. is indebted to the Deutscher Akademischer Austausch Dienst (DAAD) for a scholarship funding. We thank Arne Helth and Matthias Bönisch for helpful discussions.

■ REFERENCES

(1) Armand, M. Issues and challenges facing rechargeable lithium batteries. *Nature* **2001**, *414*, 359−367.

(2) Scrosati, B. Lithium rocking chair batteries: An old concept? History of rocking chair batteries. *J. Electrochem. Soc.* **1992**, *139*, 2776−2781.

(3) Zhu, C.; Xia, X.; Liu, J.; Fan, Z.; Chao, D.; Zhang, H.; Fan, H. J. TiO_2 nanotube@SnO_2 nanoflake core−branch arrays for lithium-ion battery anode. *Nano Energy* **2014**, *4*, 105−112.

(4) Wei, Z.; Liu, Z.; Jiang, R.; Bian, C.; Huang, T.; Yu, A. TiO_2 nanotube array film prepared by anodization as anode material for lithium ion batteries. *J. Solid State Electrochem.* **2009**, *14*, 1045−1050.

(5) Wang, Y.; Liu, S.; Huang, K.; Fang, D.; Zhuang, S. Electrochemical properties of freestanding TiO_2 nanotube membranes annealed in Ar for lithium anode material. *J. Solid State Electrochem.* **2011**, *16*, 723−729.

(6) Mancini, M.; Nobili, F.; Tossici, R.; Wohlfahrt-Mehrens, M.; Marassi, R. High performance, environmentally friendly and low cost anodes for lithium-ion battery based on TiO_2 anatase and water soluble binder carboxymethyl cellulose. *J. Power Sources* **2011**, *196*, 9665−9671.

(7) Hassoun, J.; Pfanzelt, M.; Kubiak, P.; Wohlfahrt-Mehrens, M.; Scrosati, B. An advanced configuration TiO_2/$LiFePO_4$ polymer lithium ion battery. *J. Power Sources* **2012**, *217*, 459−463.

(8) Han, H.; Song, T.; Lee, E.-K.; Devadoss, A.; Jeon, Y.; Ha, J.; Chung, Y.-C.; Choi, Y.-M.; Jung, Y.-G.; Paik, U. Dominant factors governing the rate capability of a TiO_2 nanotube anode for high power lithium ion batteries. *ACS Nano* **2012**, *6*, 8308−8315.

(9) Guan, D.; Cai, C.; Wang, Y. Amorphous and crystalline TiO_2 nanotube arrays for enhanced Li-ion intercalation properties. *J. Nanosci. Nanotechnol.* **2011**, *11*, 3641−3650.

(10) Earle, M. D. The electrical conductivity of titanium dioxide. *Phys. Rev.* **1942**, *61*, 56−62.

(11) Yoon, S.; Ka, B. H.; Lee, C.; Park, M.; Oh, S. M. Preparation of nanotube TiO_2-carbon composite and its anode performance in lithium-ion batteries. *Electrochem. Solid-State Lett.* **2009**, *12*, A28.

(12) Su, X.; Wu, Q.; Zhan, X.; Wu, J.; Wei, S.; Guo, Z. Advanced titania nanostructures and composites for lithium ion battery. *J. Mater. Sci.* **2012**, *47*, 2519−2534.

(13) Rai, A. K.; Anh, L. T.; Gim, J.; Mathew, V.; Kang, J.; Paul, B. J.; Song, J.; Kim, J. Simple synthesis and particle size effects of TiO_2 nanoparticle anodes for rechargeable lithium ion batteries. *Electrochim. Acta* **2013**, *90*, 112−118.

(14) Shankar, K.; Basham, J. I.; Allam, N. K.; Varghese, O. K.; Mor, G. K.; Feng, X.; Paulose, M.; Seabold, J. A.; Choi, K.-S.; Grimes, C. A. Recent advances in the use of TiO_2 nanotube and nanowire arrays for oxidative photoelectrochemistry. *J. Phys. Chem. C* **2009**, *113*, 6327−6359.

(15) Kubiak, P.; Geserick, J.; Hüsing, N.; Wohlfahrt-Mehrens, M. Electrochemical performance of mesoporous TiO_2 anatase. *J. Power Sources* **2008**, *175*, 510−516.

(16) Kubiak, P.; Fröschl, T.; Hüsing, N.; Hörmann, U.; Kaiser, U.; Schiller, R.; Weiss, C. K.; Landfester, K.; Wohlfahrt-Mehrens, M. TiO_2 anatase nanoparticle networks: Synthesis, structure, and electrochemical performance. *Small* **2011**, *7*, 1690−1696.

(17) Guo, Y. G.; Hu, Y. S.; Sigle, W.; Maier, J. Superior electrode performance of nanostructured mesoporous TiO_2 (anatase) through efficient hierarchical mixed conducting networks. *Adv. Mater.* **2007**, *19*, 2087−2091.

(18) Cao, F.; Wu, X.; Xin, S.; Guo, Y.; Wan, L. Facile synthesis of mesoporous TiO_2−C nanosphere as an improved anode material for superior high rate 1.5 V rechargeable Li ion batteries containing $LiFePO_4$−C cathode. *J. Phys. Chem. C* **2010**, *114*, 10308−10313.

(19) Cao, F. F.; Guo, Y. G.; Zheng, S. F.; Wu, X. L.; Jiang, L. Y.; Bi, R. R.; Wan, L. J.; Maier, J. Symbiotic coaxial nanocables: Facile synthesis and an efficient and elegant morphological solution to the lithium storage problem. *Chem. Mater.* **2010**, *22*, 1908−1914.

(20) Wu, Q. L.; Li, J.; Deshpande, R. D.; Subramanian, N.; Rankin, S. E.; Yang, F.; Cheng, Y. Aligned TiO_2 nanotube arrays as durable lithium-ion battery negative electrodes. *J. Phys. Chem. C* **2012**, *116*, 18669−18677.

(21) Liu, D.; Xiao, P.; Zhang, Y.; Garcia, B. B.; Zhang, Q.; Guo, Q.; Champion, R.; Cao, G. TiO_2 nanotube arrays annealed in N_2 for efficient lithium-ion intercalation. *J. Phys. Chem. C* **2008**, 11175−11180.

(22) Lu, Z.; Yip, C.-T.; Wang, L.; Huang, H.; Zhou, L. Hydrogenated TiO_2 nanotube arrays as high-rate anodes for lithium-ion microbatteries. *ChemPlusChem* **2012**, *77*, 991−1000.

(23) Tang, Y.; Liu, Z.; Lü, X.; Wang, B.; Huang, F. TiO_2 nanotubes grown on graphene sheets as advanced anode materials for high rate lithium ion batteries. *RSC Adv.* **2014**, *4*, 36372.

(24) Guan, D.; Li, J.; Gao, X.; Yuan, C. Controllable synthesis of MoO_3-deposited TiO_2 nanotubes with enhanced lithium-ion intercalation performance. *J. Power Sources* **2014**, *246*, 305−312.

(25) Allam, N. K.; Deyab, N. M.; Abdel Ghany, N. Ternary Ti-Mo-Ni mixed oxide nanotube arrays as photoanode materials for efficient solar hydrogen production. *Phys. Chem. Chem. Phys.* **2013**, *15*, 12274−12282.

(26) Jo, C.-I.; Jeong, Y.-H.; Choe, H.-C.; Brantley, W. A. Hydroxyapatite precipitation on nanotubular films formed on Ti-6Al-4V alloy for biomedical applications. *Thin Solid Films* **2013**, *549*, 135−140.

(27) Mor, G. K.; Prakasam, H. E.; Varghese, O. K.; Shankar, K.; Grimes, C. A. Vertically oriented Ti-Fe-O nanotube array films: Toward a useful material architecture for solar spectrum water photoelectrolysis. *Nano Lett.* **2007**, *7*, 2356−2364.

(28) Yang, Y.; Kim, D.; Schmuki, P. Electrochromic properties of anodically grown mixed V_2O_5−TiO_2 nanotubes. *Electrochem. Commun.* **2011**, *13*, 1021−1025.

(29) Kim, J.-H.; Zhu, K.; Yan, Y.; Perkins, C. L.; Frank, A. J. Microstructure and pseudocapacitive properties of electrodes constructed of oriented NiO-TiO_2 nanotube arrays. *Nano Lett.* **2010**, *10*, 4099−4104.

(30) Thomas, J. H. Electrical properties of thin cobalt oxide films on cobalt. *Thin Solid Films* **1977**, *44*, 155−161.

DOI: 10.1021/acssuschemeng.5b00026
ACS Sustainable Chem. Eng. 2015, 3, 909−919

(31) Lange, F.; Martin, M. The electrical conductivity of CoO: Experimental results and a new conductivity model. *Ber. Bunsenges. Phys. Chem.* **1997**, *101*, 176−184.
(32) Persels Constant, K.; Mason, T. O.; Rothman, S. J.; Routbort, J. L. Non-stoichimetry, electrical properties, and cation diffusion in highly non-stoichimetric $Co_{1-x}O$—I. Experimental. *J. Phys. Chem. Solids* **1992**, *53*, 405−411.
(33) Hübener, K.; Leonhardt, G. Ionicity and electrical conductivity in transition-metal oxides. *Phys. Status Solidi B* **1975**, *68*, K175−K179.
(34) Joshi, G. M.; Pai, M.; Harrison, H. R.; Sandberg, C. J.; Aragón, R.; Honig, J. M. Electrical properties of undoped single CoO crystals. *Mater. Res. Bull.* **1980**, *15*, 1575−1579.
(35) Fan, Y.; Zhang, N.; Zhang, L.; Shao, H.; Wang, J.; Zhang, J.; Cao, C. Co_3O_4-coated TiO_2 nanotube composites synthesized through photo-deposition strategy with enhanced performance for lithium-ion batteries. *Electrochim. Acta* **2013**, *94*, 285−293.
(36) Cao, C.; Hu, C.; Shen, W.; Wang, S.; Liu, H.; Wang, J. Cobalt oxide modified highly ordered TiO_2 nanotube arrays: Enhanced visible light photoelectrochemical properties. *Sci. Adv. Mater.* **2013**, *5*, 1256−1263.
(37) Stoica, E.-D.; Fedorov, F.; Nicolae, M.; Uhlemann, M.; Gebert, A.; Schultz, L. Ti6Al7Nb surface modification by anodization in electrolytes containing HF. *Sci. Bull. - Univ. "Politeh." Bucharest, Ser. B* **2012**, *74*, 277−288.
(38) Burgers, W. G.; Jacobs, F. M. Crystal structure of β-titanium. *Z. Kristallogr.* **1936**, *94*, 299−300.
(39) Skripov, A. V.; Buzlukov, A. L.; Soloninin, A. V.; Voronin, V. I.; Berger, I. F.; Udovic, T. J.; Huang, Q.; Rush, J. J. Hydrogen motion and site occupation in $Ti_2CoH_x(D_x)$: NMR and neutron scattering studies. *Physica B* **2007**, *392*, 353−360.
(40) Patterson, A. Crystal structure of titanium and chromium. *Phys. Rev.* **1925**, *25*, 56−58.
(41) Chebotareva, E. S.; Nuzhdina, S. G. Observation of ω-titanium in a composite hard facing alloy based on fine-grain diamonds. *Phys. Met. Metallogr.* **1973**, *36*, 200−202.
(42) Murray, J. L. The Co-Ti (cobalt-titanium) system Co-Ti. *Bull. Alloy Phase Diagrams* **1982**, *3*, 74−85.
(43) Ferreira, C. P.; Gonçalves, M. C.; Caram, R.; Bertazzoli, R.; Rodrigues, C. A. Effects of substrate microstructure on the formation of oriented oxide nanotube arrays on Ti and Ti alloys. *Appl. Surf. Sci.* **2013**, *285*, 226−234.
(44) Saji, V. S.; Choe, H. C.; Brantley, W. A. Nanotubular oxide layer formation on Ti-13Nb-13Zr alloy as a function of applied potential. *J. Mater. Sci.* **2009**, *44*, 3975−3982.
(45) Kim, W. G.; Choe, H. C.; Ko, Y. M.; Brantley, W. A. Nanotube morphology changes for Ti-Zr alloys as Zr content increases. *Thin Solid Films* **2009**, *517*, 5033−5037.
(46) Zarco, V. I.; Gette, A. V.; Kozub, G. M.; Sushko, R. V.; Chuiko, A. A. Structural and electrophysical characteristics of titanium-containing silicon dioxide. *Inorg. Mater.* **1983**, *19*, 215−217.
(47) Sakata, K. Study of the phase transition in $Nb_xTi_{1-x}O_2$. *J. Phys. Soc. Jpn.* **1969**, *26*, 1067.
(48) Dorémieux, J. L.; Poilblanc, R. Sur la présence de restes acétates dans un composé chimiquement proche de CoO. *C. R. Seances Acad. Sci., Ser. C* **1967**, *264*, 1278−1281.
(49) Legrand, C.; Delville, J. Sur les paramètres cristallins du rutile et del'anatase. *C. R. Hebd. Seances Acad. Sci.* **1953**, *236*, 944−946.
(50) Fierro, G.; Lo Jacono, M.; Inversi, M.; Dragone, R.; Porta, P. TPR and XPS study of cobalt−copper mixed oxide catalysts: Evidence of a strong Co−Cu interaction. *Top. Catal.* **2000**, *10*, 39−48.
(51) Barreca, D.; Massignan, C.; Daolio, S.; Fabrizio, M.; Piccirillo, C.; Armelao, L.; Tondello, E. Composition and microstructure of cobalt oxide thin films obtained from a novel cobalt(II) precursor by chemical vapor deposition. *Chem. Mater.* **2001**, *13*, 588−593.
(52) Roy, P.; Berger, S.; Schmuki, P. TiO_2 nanotubes: Synthesis and applications. *Angew. Chem., Int. Ed.* **2011**, *50*, 2904−2939.
(53) Bauer, S.; Kleber, S.; Schmuki, P. TiO_2 nanotubes: Tailoring the geometry in H_3PO_4/HF electrolytes. *Electrochem. Commun.* **2006**, *8*, 1321−1325.
(54) Esquivel, K.; García, J. M. G.; Rodríguez, F. J.; González, M. V.; Escobar-Alarcón, L.; Ortiz-Frade, L.; Godínez, L. A. Titanium dioxide doped with transition metals ($MTi_{1-x}O_2$, M: Ni, Co): Synthesis and characterization for its potential application as photoanode. *J. Nanoparticle Res.* **2011**, *13*, 3313−3325.
(55) Hardcastle, F. D. Raman spectroscopy of titania (TiO_2) nanotubular water-splitting catalysts. *J. Arkansas Acad. Sci.* **2011**, *65*, 43−48.
(56) Yu, Y.; Yu, J. C.; Yu, J.-G.; Kwok, Y.-C.; Che, Y.-K.; Zhao, J.-C.; Ding, L.; Ge, W.-K.; Wong, P.-K. Enhancement of photocatalytic activity of mesoporous TiO_2 by using carbon nanotubes. *Appl. Catal., A* **2005**, *289*, 186−196.
(57) Tang, C. W.; Wang, C. B.; Chien, S. H. Characterization of cobalt oxides studied by FT-IR, Raman, TPR and TG-MS. *Thermochim. Acta* **2008**, *473*, 68−73.
(58) Choi, H. C.; Jung, Y. M.; Noda, I.; Kim, S. B. A study of the mechanism of the electrochemical reaction of lithium with CoO by two-dimensional soft X-ray absorption spectroscopy (2D XAS), 2D Raman, and 2D heterospectral XAS-Raman correlation analysis. *J. Phys. Chem. B* **2003**, *107*, 5806−5811.
(59) Ma, H. L.; Yang, J. Y.; Dai, Y.; Zhang, Y. B.; Lu, B.; Ma, G. H. Raman study of phase transformation of TiO_2 rutile single crystal irradiated by infrared femtosecond laser. *Appl. Surf. Sci.* **2007**, *253*, 7497−7500.
(60) Koudriachova, M.; Harrison, N.; de Leeuw, S. Effect of diffusion on lithium intercalation in titanium dioxide. *Phys. Rev. Lett.* **2001**, *86*, 1275−1278.
(61) Deng, D.; Kim, M. G.; Lee, J. Y.; Cho, J. Green energy storage materials: Nanostructured TiO_2 and Sn-based anodes for lithium-ion batteries. *Energy Environ. Sci.* **2009**, *2*, 818.
(62) Paulose, M.; Shankar, K.; Yoriya, S.; Prakasam, H. E.; Varghese, O. K.; Mor, G. K.; Latempa, T. A.; Fitzgerald, A.; Grimes, C. A.; Park, U. V.; et al. Anodic growth of highly ordered TiO_2 nanotube arrays to 134 μm in length. *J. Phys. Chem. B* **2006**, *110*, 16179−16184.
(63) Bavykin, D. V.;Walsh, F. C. *Titanate and Titania Nanotubes*; Royal Society of Chemistry: Cambridge, 2009.
(64) Ortiz, G. F.; Hanzu, I.; Lavela, P.; Knauth, P.; Tirado, J. L.; Djenizian, T. Nanoarchitectured TiO_2/SnO: A future negative electrode for high power density Li-ion microbatteries? *Chem. Mater.* **2010**, *22*, 1926−1932.
(65) Ivanov, S.; Cheng, L.; Wulfmeier, H.; Albrecht, D.; Fritze, H.; Bund, A. Electrochemical behavior of anodically obtained titania nanotubes in organic carbonate and ionic liquid based Li ion containing electrolytes. *Electrochim. Acta* **2013**, *104*, 228−235.
(66) Kim, J.-H.; Zhu, K.; Kim, J. Y.; Frank, A. J. Tailoring oriented TiO_2 nanotube morphology for improved Li storage kinetics. *Electrochim. Acta* **2013**, *88*, 123−128.
(67) Zhu, K.; Wang, Q.; Kim, J.; Pesaran, A. A.; Frank, A. J. Pseudocapacitive lithium-ion storage in oriented anatase TiO_2 nanotube arrays. *J. Phys. Chem. C* **2012**, *116*, 11895−11899.
(68) Wang, Y.; Liu, S.; Huang, K.; Fang, D.; Zhuang, S. Electrochemical properties of freestanding TiO_2 nanotube membranes annealed in Ar for lithium anode material. *J. Solid State Electrochem.* **2011**, *16*, 723−729.

DOI: 10.1021/acssuschemeng.5b00026
ACS Sustainable Chem. Eng. 2015, 3, 909−919